International Journal of Fracture **73**: 67–79, 1995.

Dynamic fracture detection using the force-displacement reciprocity: application to the compact compression specimen

H. MAIGRE and D. RITTEL*
Laboratoire de Mécanique des Solides, U.R.A. 317-C.N.R.S., Ecole Polytechnique, F-91128 Palaiseau Cedex, France

Received 12 January 1994; accepted 1 January 1995

Abstract. Dynamic fracture toughness is determined by impacting fracture specimens and determining the onset of crack propagation. In such experiments characteristic impedance (actuator-specimen) matching problems can affect the accuracy of the measured forces. In addition, fracture time is mostly determined by means of surface rather than bulk devices (e.g. gages). In this paper we address these issues in linear-elastic materials. Based on the H-integral we show that *either* the measured forces *or* the displacements (whichever is more accurate) can be used to calculate the evolutions of the stress intensity factors. These evolutions must be identical by virtue of the reciprocity between forces and displacements, at least until some bulk fracture process develops. Examples are presented to illustrate how these observations can be applied to 'fine-tune' dynamic fracture experiments and complement fracture gage readings.

1. Introduction

Dynamic fracture testing of materials is a delicate problem both theoretically and experimentally. The theoretical difficulties are related to inertial effects which do not exist for statically applied loads [1]. Most of the experimental activity in that field is concerned with the determination of the dynamic stress intensity factors (SIF). Typical experiments generally involve sophisticated techniques and sometimes intensive numerical calculations (see *e.g.* review [2] and [3]).

Recently, a new approach has been introduced which comprises theoretical, experimental as well as numerical aspects [4–6]. Knowledge of the forces *and* displacements on the boundaries of a cracked specimen is sufficient to completely determine the evolutions of the dynamic stress intensity factors thanks to the path independent H-integral. To that matter, a new fracture specimen (the Compact Compression Specimen-CCS) has been especially devised to be easily inserted in standard Kolsky (split Hopkinson) bars. Furthermore, the degree of mode mixity – a crucial problem in dynamic fracture testing [7] – has also been characterized for this experiment [8].

The degree of accuracy of the stress intensity factors depends chiefly on the precision achieved in assessing the forces and the displacements at the specimen's boundaries as well as the time at which the crack starts to propagate. The purpose of this paper is to address experimental precision by presenting new results for the CCS technique which apply also to general dynamic fracture toughness testing. In Section 2, we briefly recall the principle of the CCS technique and the main results obtained so far. In Section 3, we discuss the reciprocity between forces and displacements. Specifically, we show how this reciprocity can be used for

* Present address: Faculty of mechanical engineering, technion, 32000 Haifa, Israel.

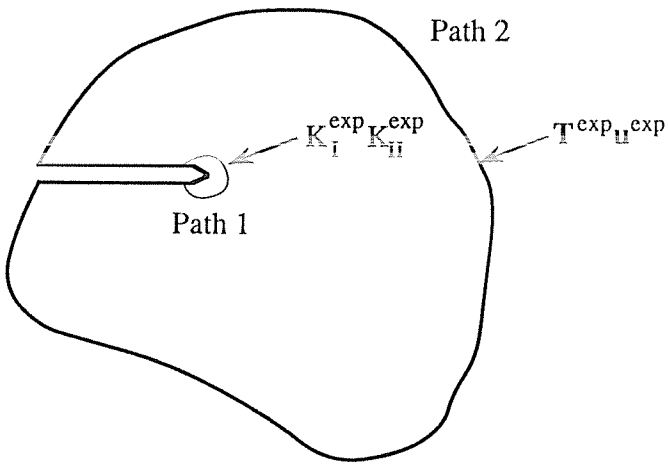

Fig. 1. Two specific contours for the evaluation of the H-integral.

a better interpretation of experimental results. Next, we address the issue of surface *vs.* bulk detection of the onset of crack propagation and show specific examples. Finally, in Section 4, we draw conclusions which apply to general dynamic fracture toughness testing practice.

2. The H-integral and the CCS technique

$H(t)$ is a path-independent integral which combines *experimental* and *reference* fields (forces $\mathbf{T}^{\text{exp}}(t)$, $\mathbf{T}^{\text{ref}}(t)$ and displacements $\mathbf{u}^{\text{exp}}(t)$, $\mathbf{u}^{\text{ref}}(t)$) through time convolution products (boldface characters indicate vectors) [4, 5]. It should be emphasized that this concept applies to two-dimensional deformations and linear elastic materials. Furthermore it is valid from the application of the load until the onset of crack propagation only. In other words, the present framework rules out crack propagation and nonlinear constitutive laws.

Two different specific integration paths can be chosen for the evaluation of H: the first along the external boundary of the structure, and the second in the vicinity of the crack tip (Fig. 1).

The expression for $H(t)$ evaluated along the boundary of a structure containing a crack of length a is given by

$$H(t) := \frac{1}{2}\int_s \left\{ \mathbf{T}^{\text{exp}} * \frac{\partial \mathbf{u}^{\text{ref}}}{\partial \mathbf{a}} - \frac{\partial \mathbf{T}^{\text{ref}}}{\partial \mathbf{a}} * \mathbf{u}^{\text{exp}} \right\} \mathrm{d}S, \tag{1a}$$

where $*$ denotes time convolution product ($[\mathbf{A} * \mathbf{B}](\tau) = \int_0^\tau \sum_i \{A_i(t)B_i(\tau - t)\}\mathrm{d}t$).

In the vicinity of the crack tip, the general expression of $H(t)$ under plane strain conditions involves both mode I and II stress intensity factors (K_{Id} and K_{IId}) for arbitrary loading

$$H(t) := H_{\text{I}}(t) + H_{\text{II}}(t) = \frac{1-\nu^2}{E}\{K_{\text{Id}}^{\text{exp}} * K_{\text{Id}}^{\text{ref}} + K_{\text{IId}}^{\text{exp}} * K_{\text{IId}}^{\text{ref}}\}, \tag{1b}$$

(E and ν are Young's modulus and Poisson's ratio respectively).

The H-integral relates *global* information – forces and displacements – collected on the boundary of the structure to *local* – crack tip – stress intensity factors. The reference

displacement field can be chosen to enforce either pure mode I or pure mode II. In each case, the determination of the evolution of the stress intensity factor amounts to solving a scalar linear convolution equation of the type

$$K_{id}^{\exp} * K_{id}^{\mathrm{ref}} = H_i(t; \{\mathbf{T}, \mathbf{u}\}^{\exp}, \{\mathbf{T}, \mathbf{u}\}^{\mathrm{ref}}) \qquad i = I \,\mathrm{or}\, II. \tag{2}$$

Consequently, for practical applications one needs the following:

- Determine a cracked specimen geometry and the adequate setup to measure both loads ($\mathbf{T}^{\exp}$) and displacements ($\mathbf{u}^{\exp}$) on its boundaries.
- Generation of reference fields $\mathbf{T}^{\mathrm{ref}}$ and $\mathbf{u}^{\mathrm{ref}}$. These fields are arbitrary and we calculate them numerically. For a given geometry, this is done *once for all* per mode for any combination of loading and crack length between a and $a + \mathrm{d}a$.
- A solver for scalar linear convolution equations.

The experimental setup we use is a standard Kolsky apparatus [9]. This apparatus is often used for dynamic compression tests and determination of dynamic stress strain curves. In this context, we will only note that the Kolsky apparatus is a convenient means to apply and measure transient loads and displacements on the boundaries of a specimen sandwiched between the bars. The specimen geometry we adopted is shown in Fig. 2. This specimen (the Compact Compression Specimen, CCS) was designed especially to be inserted between the incident and transmitter bars. This geometry eliminates the need for additional fixtures which cause crack opening upon compressive loading (*e.g.*, compression to tension inverting devices). The specimen geometry is somewhat complex (and compact) so that numerical (FE) calculations rather than analytical means must be employed to generate references. The calculations are kept to a minimum level of complexity since there are no such fixtures to model numerically. A single wire fracture gage (MM model CD 02 15A) is glued on each specimen's face, as close as possible to the crack tip, to signal the onset of crack propagation. The crack tip can be machined or sharpened by fatigue cracking using a standard compressive machine. The fracture toughness is thus the value of the stress intensity factor at the onset of crack extension.

Despite the symmetry of the CCS, the loading is not symmetrical so that the forces on face 1 (incident) and face 2 (transmitter) are neither equal nor synchronized (Fig. 3). Consequently, mixed I-II crack opening mode develops. The extent of mode mixity was characterized and it was observed that for a typical experiment, the crack starts to propagate under dominant mode I [8, 10].

3. On the reciprocity of forces and displacements

The general expression for the H-integral involves both forces and displacements terms by analogy with Betti's theorem in elastodynamics [1]. Whereas the force-displacement reciprocity has long been recognized, it has been so far of little practical use in experimental applications. In our experimental setup, we measure *both* the forces and the displacements at the specimen-bars interfaces. This information is quite precious to 'fine tune' the experiments as will be shown next.

A common practice in dynamic fracture experiments is to record the forces to be used as an input for a numerical calculation of the SIF (see *e.g.* [11]). In our case, this amounts to

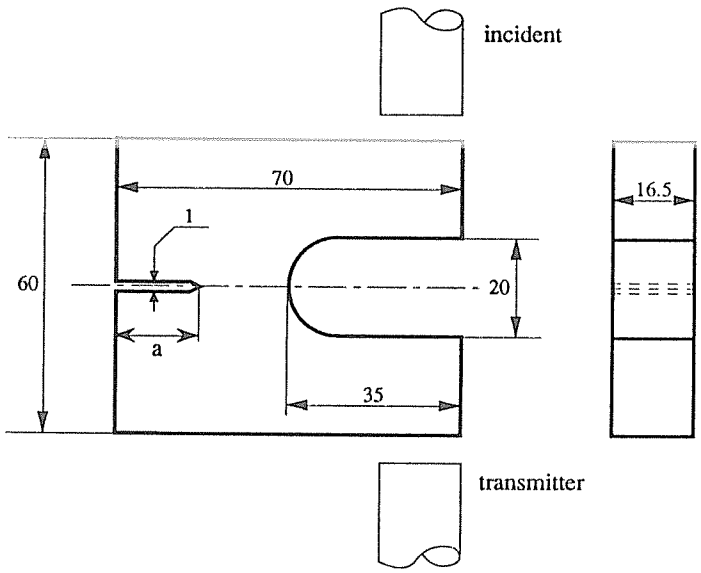

Fig. 2. The Compact Compression Specimen (all dimensions are in mm). The incident and transmitter bars are sketched to point to the CCS-bars interfaces where transient forces-displacements are applied and measured.

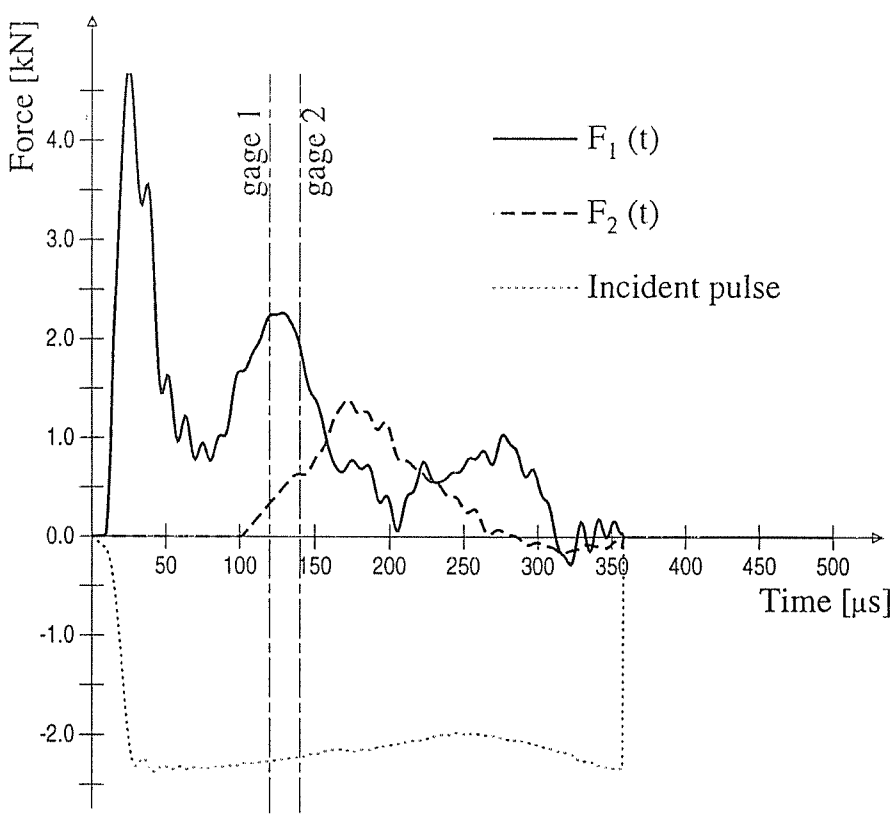

Fig. 3. Typical applied transient forces (PMMA specimen). Note the lack of symmetry of the incident (1) and transmitted (2) pulses.

keeping the reference force $\mathbf{T}^{\text{ref}}$ constant with the crack length a (*i.e.* $\frac{\partial \mathbf{T}^{\text{ref}}}{\partial \mathbf{a}} = 0$). The lhs of (1a) thus reads

$$H(t) = \frac{1}{2} \int_s \mathbf{T}^{\text{exp}} * \frac{\partial \mathbf{u}^{\text{ref}}}{\partial a} \mathrm{d}s. \tag{3a}$$

Here, we use the experimental force $\mathbf{T}^{\text{exp}}$ and its convolution with the derivative of the reference displacement field $\mathbf{u}^{\text{ref}}$ with respect to the crack length. The latter is calculated by imposing the same arbitrary force pulse and calculating the corresponding displacements for two slightly different crack lengths using FE technique [5].

Alternatively, one can choose an imposed reference displacement $\mathbf{u}^{\text{ref}}$ which remains constant with the crack length a (*i.e.* $\frac{\partial \mathbf{u}^{\text{ref}}}{\partial a} = 0$). The lhs of (1a) now reads

$$H(t) = \frac{1}{2} \int_s -\frac{\partial \mathbf{T}^{\text{ref}}}{\partial a} * \mathbf{u}^{\text{exp}} \, \mathrm{d}S. \tag{3b}$$

Here, we use the experimental displacement $\mathbf{u}^{\text{exp}}$ and its convolution with the derivative of the resultant force with respect to the crack length. By analogy with the previous case, we impose the same displacement field $\mathbf{u}^{\text{ref}}$ and calculate the resultant force for two slightly different crack lengths.

One important remark needs to be formulated. Expressions (1) and (3) are strictly equivalent. The common choice of type (3a) formulation is a matter of pure convenience which is generally dictated by the numerical algorithms involved and their relative complexity (for either prescribed forces or prescribed displacements boundary value problems) [12,13]. However, regardless of the chosen expression, the H-integral remains equal to the convolution product of the stress intensity factors (2). This issue will now be addressed further in its experimental aspects.

3.1. 'Fine tuning' of an experiment

In typical experiments with Kolsky bars three characteristic transient signals are recorded from the gages: the incident ε_{in} and reflected ε_{ref} signals (incident bar), and the transmitted ε_{tr} signal (transmitter bar). These signals can be converted into interfacial (CCS-bars) velocities and forces. The interfacial velocities are given by [9,14]

$$\begin{cases} v_1 = c_L[\varepsilon_{\text{in}} - \varepsilon_{\text{ref}}] \\ v_2 = c_L \varepsilon_{\text{tr}}, \end{cases} \tag{4a}$$

where v_1 and v_2 are input (incident) and output (transmitter) velocities respectively, c_L denotes longitudinal sound velocity in the bars.

The interfacial forces are given by

$$\begin{cases} P_1 = EA[\varepsilon_{\text{in}} + \varepsilon_{\text{ref}}] \\ P_2 = EA\varepsilon_{\text{tr}}, \end{cases} \tag{4b}$$

where A is the cross-sectional area of the bar.

Two important factors affect the quality of the results. The first is the nature of the contact between the bars and the specimen. As long as the overall flexure of the CCS's arms remains small, *i.e.* for early fracture, the contact can be assumed to be good ensuring a good transmission of the stress wave. The second relates to the relative amount of reflected and transmitted signal. This ratio depends on the characteristic impedances (ρc_L) of the bars and the material and/or structure tested [15]. In our case we refer more to a structure than to a material due to the shape of the CCS which further complicates impedance matching. This limits in turn the degree of precision attainable for $P_i (i = 1, 2)$, mostly when the incident and reflected signals reach comparable amplitudes. In such a case, it may be desirable to use the experimental displacements (3b) rather than the forces (3a). In other cases, *either* forces *or* displacements can be used and results compared. However, since both formulations must yield similar evolutions of the SIF's one can assess the nature of the contact and the extent of impedance mismatch effects. As a practical consequence, if the two evolutions diverge from the very beginning of the experiment this surely indicates an experimental problem such as lack of contact between the specimen and the bars. The choice of the formulation is thus left to the engineering judgement of the experimentalist.

In the sequel, we develop further the use of the reciprocity between forces and displacements.

3.2. Bulk vs. surface detection of crack propagation

Detection of the onset of crack propagation is central to almost all experimental techniques aiming to measure the dynamic fracture toughness. Furthemore, it also determines the extent of mode mixity [7, 8]. In our experiments, fracture time is signalled by means of single wire fracture gages glued on each side of the specimen as close as possible to the crack tip. Several factors can affect the accuracy of this measurement.

The distance between the gages and the crack tip is ascertained after fracture and is typically found to be around 5×10^{-4} m. For typical crack velocities (300 to 1000 m/s) this will only cause a small delay between the onset of crack propagation and its detection. Yet, in many cases, the gage readings can indicate different times due not only to misplacement but also to uneven through the thickness crack front.

An additional issue is related to the nature of the fracture process: where does the first 'event' (*e.g.* microcrack) leading to crack formation occur with respect to the surface gages or other detection device? In other words, what is the relationship between bulk crack initiation and surface detection? While little experimental information is available on that matter, a recent numerical simulation of the optical method of caustics has addressed certain aspects of this problem [16].

Keeping in mind that the CCS technique is based on a 2D representation of an actual 3D process, it is realized that the measured fracture toughness is equivalent to a thickness averaged value of the actual fracture toughness of the material (by analogy with static fracture toughness determination). As mentioned previously, using *both* the recorded forces and displacements in (3a) and (3b) must yield identical evolutions of the stress intensity factors until loss of reciprocity. This corresponds to some fracture process being initiated ahead of the main crack. The time at which this occurs can be considered as the corresponding bulk averaged fracture time, as will be shown next.

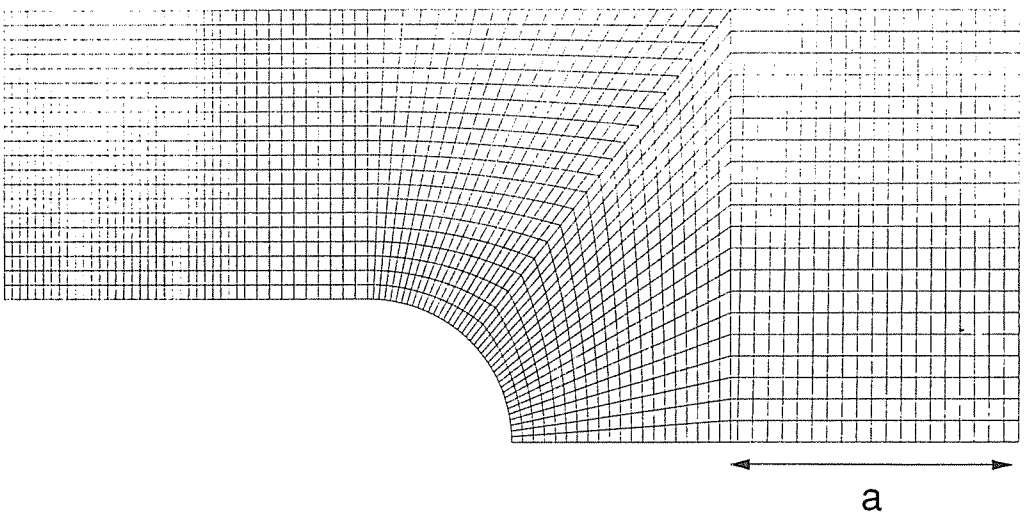

Fig. 4. Half a CCS discretized for explicit FE calculations.

3.3. Dynamic fracture toughness of a commercial hard steel and PMMA

3.3.1. *Numerical procedure*

In previous work [5,6,8], we generated reference data with an implicit procedure which is unconditionally stable [12]. Here we used an explicit (central differences) scheme for the direct integration of the equations of equilibrium with a diagonalized mass matrix. Two specific types of boundary conditions were imposed

- imposed force pulse $\mathbf{T}_i^{\text{ref}}$ to calculate the derivative of the displacements $\frac{\partial \mathbf{u}_i^{\text{ref}}}{\partial a}$ $(i = I, II)$ in (3a).
- imposed displacement pulse $\mathbf{u}_i^{\text{ref}}$ to calculate the derivative of the reactions $\frac{\partial \mathbf{T}_i^{\text{ref}}}{\partial a}$ $(i = I, II)$ in (3b).

All procedures were written in the object oriented F.E. code CASTEM 2000, as in previous applications [17]. Likewise, the stress intensity factors were calculated from the displacements of a selected point using Irwin's relationship [5]. A typical meshed half-specimen is shown in Fig. 4. By comparison with previous meshes [5,6,8], this mesh is slightly coarser and more regular.

For this explicit procedure, care was excercised to maintain stability through appropriate spatial/temporal discretization along with monitoring the balance of energies [12,13]. The choice of an explicit procedure was a matter of convenience. A preliminary step was to make sure that explicit and implicit procedures give identical results when applied to the same problem. Consequently we checked for path independence of the results. This was done in mode I and in mode II by comparing the boundary and the near-tip values of the H-integral. For the boundary value we used

$\mathbf{T}^{\text{ref}} * \frac{\partial \mathbf{u}_i^{\text{ref}}}{\partial a}$ and $-\mathbf{u}^{\text{ref}} * \frac{\partial \mathbf{T}_i^{\text{ref}}}{\partial a}$, while for the crack tip value we used $K_i^{\text{ref}} * K_i^{\text{ref}} i = I, II$ [8]. As shown in Fig. 5, the present numerical procedure preserves satisfactorily the path-independent character of the H-integral. Boundary and near-tip values are in phase in both modes but the relative error on the value of H is more important in mode II than in mode I.

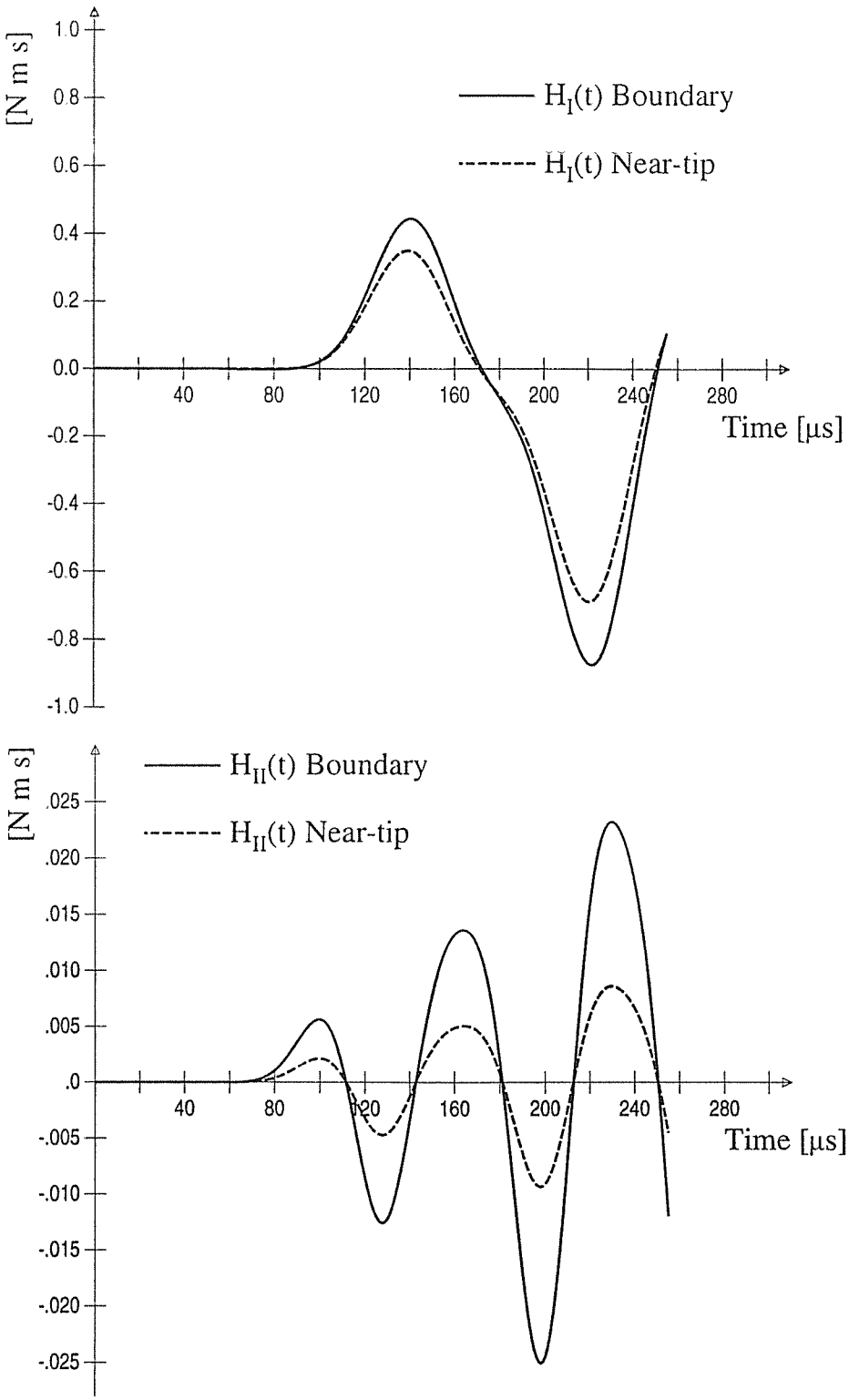

Fig. 5. Near-tip and boundary calculated values of the H-integral. (a) mode I and (b) mode II.

This is consistent with previous observations [8], and it results from the relative coarseness of the mesh together with the fact that mode I is by far the major mode. Consequently in the present study we will consider dominant mode I only.

3.3.2. *Commercial hard carbon steel*

Dynamic fracture toughness of a commercial hard carbon steel was tested using the CCS technique. Here, the impedance matching was satisfactory, resulting in a relatively small reflected wave. Therefore, the same degree of accuracy was achieved on the forces and the displacements. In this series of experiments, two fracture gages were used (one on each side of the specimen). For the first specimen, the crack was of uneven length through the thickness, 18.30 mm on side 1 and 17.02 mm on side 2 (average crack length 17.6 mm). Gage 1 was positioned at 18.3 mm and indicated fracture after 60 μs. Gage 2 was positioned at 17.39 mm (slightly beyond the crack tip) and read 68 μs. In Fig. 6a, we have plotted the evolutions of the two stress intensity factors with time. The bulk time at which the evolutions separate is slightly inferior to 60 μs.

This example represents a typical case of uneven crack length with an error on the position of the gages (which cannot be avoided beforehand). Here, the use of the redundant couple forces-displacements enables the determination of a bulk time to the fracture which is closer to the reading of gage 1. Consequently, the reading of gage 1 together with the bulk time can be considered as a sound estimate of fracture time.

For the second specimen, the crack-front was relatively straight (19.95 mm). The two gages were positioned quite close to the tip and read 66 and 70 μs respectively. From the evolutions plotted in Fig. 6b it can be noted that bulk fracture occurs before it is detected by the surface gages.

3.4. Commercial PMMA

In [10] we reported results for the dynamic fracture toughness of commercial PMMA tested under different stress intensity rates with a single fracture gage and a relatively uniform crack length. Here, by using a maraging steel bar with a PMMA sample, the impedance matching is not ideal resulting in a larger uncertainty on the experimental forces with respect to the displacements.

The evolutions of the mode I stress intensity factors (mode II is known to be minor) obtained by using experimental forces and displacements are shown in Fig. 7 (samples P6 and P10 in [10]). From this figure, it can be noted that the two evolutions are initially similar for about 80 μs. This indicates that despite the poor impedance matching, the forces and the displacements were accurately measured. Also, the bulk fracture time (divergence time) is slightly shorter than that measured by the surface gages (less than 10 μs). This result makes sense as fracture is expected to initiate in the bulk of the specimen rather than on its smooth surface. Furthermore, the consistency of these two times (bulk and gage) indicates that in this experiment, the fracture gages performed reliably. Yet, should both gages have failed to perform satisfactorily, the bulk time to fracture thus determined would still have yielded a reasonable estimate of the dynamic fracture toughness.

One remark can be made concerning the difference between the bulk fracture time and that indicated by the gages. The specimen thickness was 16.5 mm and assuming that fracture started at mid-thickness, a simple calculations shows that the average crack velocity would be

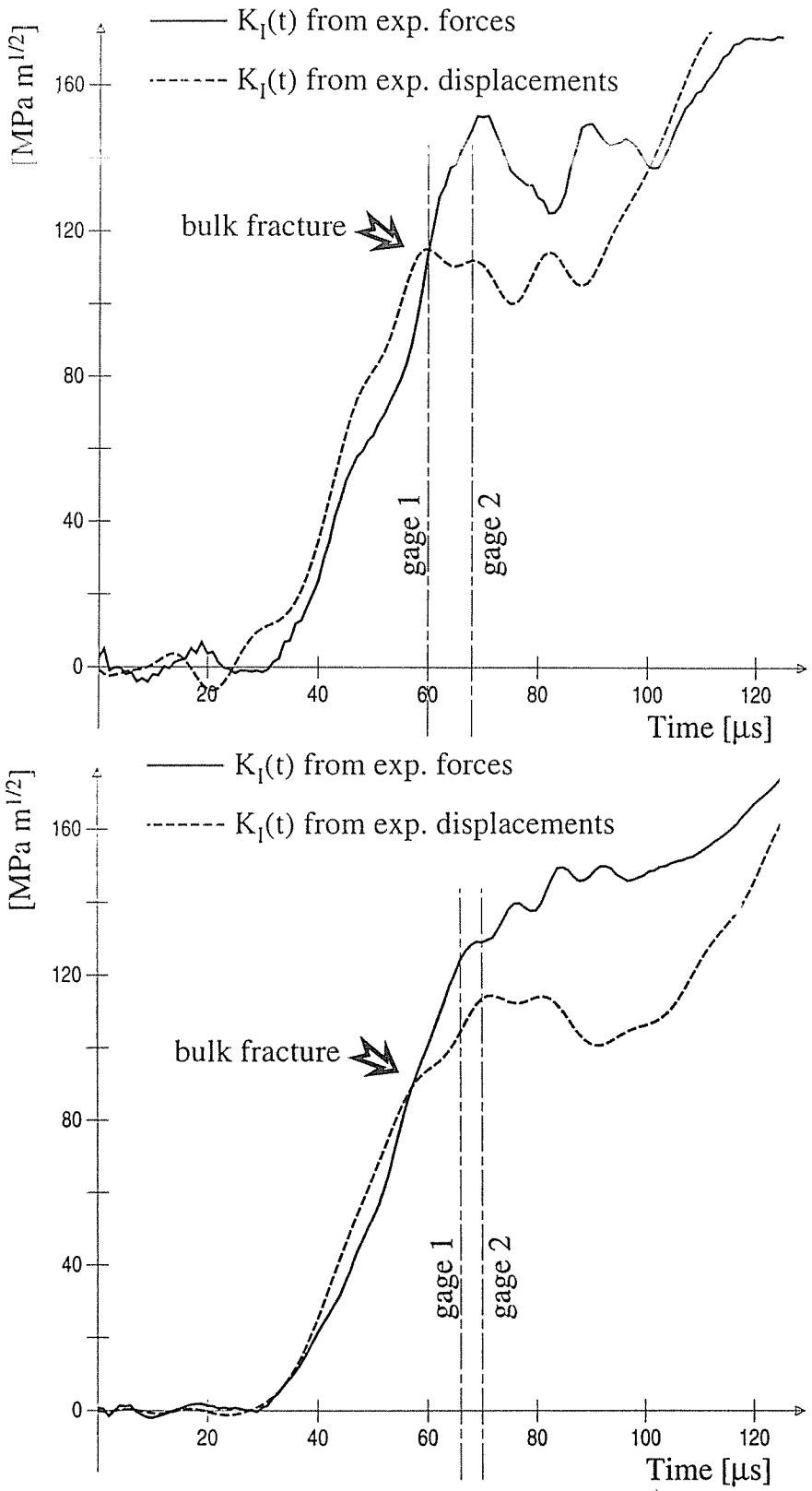

Fig. 6. Steel specimens. Evolutions of the mode I stress intensity factors calculated using once experimental forces and once experimental displacements. Both evolutions are similar until the onset of bulk fracture. Gage 1 and gage 2 indicate surface gage readings. (a) crack length between 17.02 and 18.30 mm; (b) crack length of 19.95 mm.

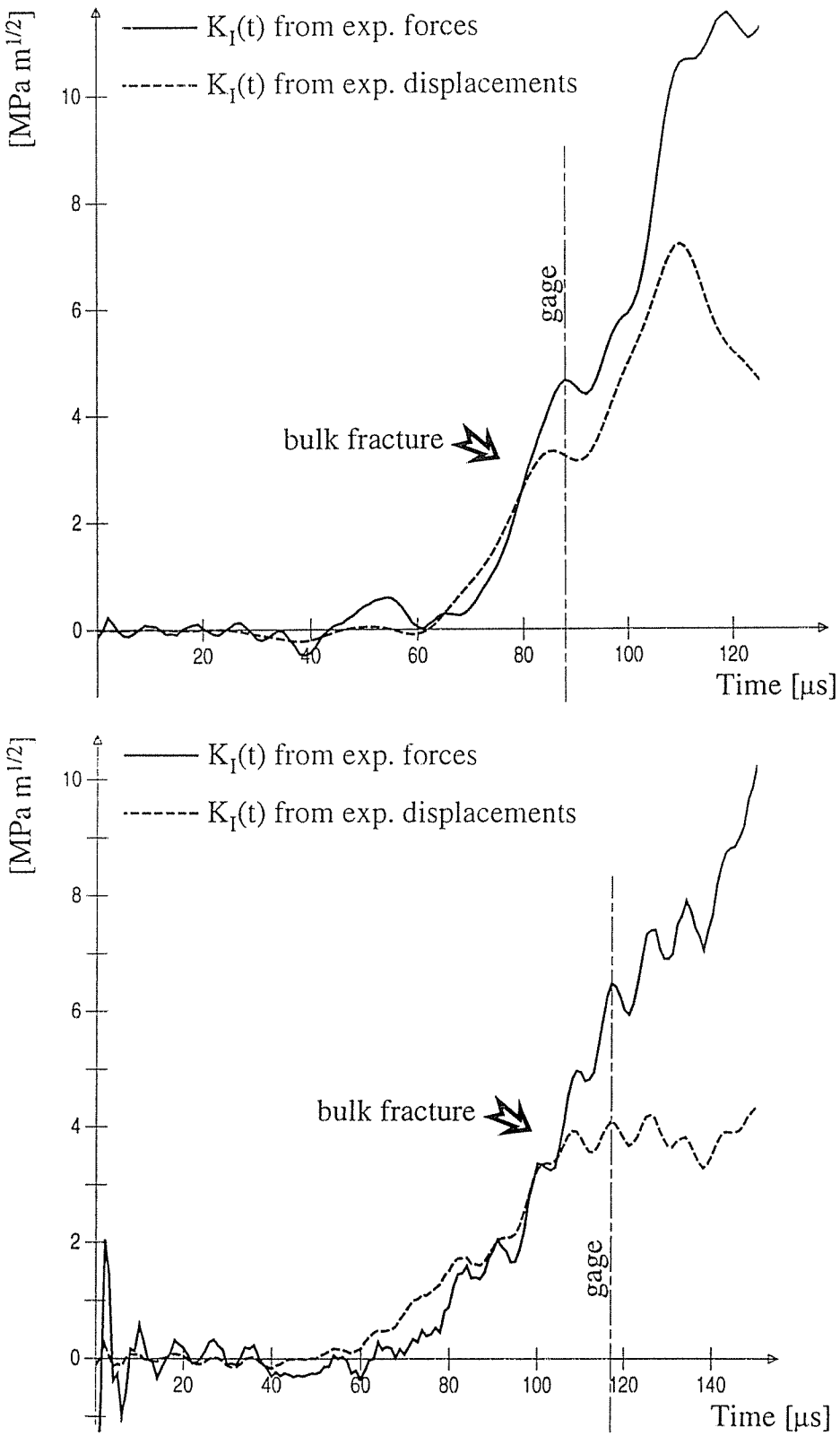

Fig. 7. PMMA specimens. Evolutions of the mode I stress intensity factors calculated using once experimental forces and once experimental displacements. (a) P6 and (b) P10 in [10].

1650 m/s. This value is of the order of the Rayleigh wave velocity in PMMA and is therefore not realistic [18]. It is thus more appropriate to assume that dynamic crack initiation involves several individual events which link up to yield one macrocrack.

4. Conclusions

This paper presents additional experimental aspects of the CCS technique for dynamic fracture toughness determination.

It has been shown that the redundant couple of data – forces *and* displacements – can be used to improve the experimental accuracy. Specifically, the evolutions of dynamic SIF's can be calculated using *either* experimental forces *or* displacements, whichever is more accurate. Both data must yield initially identical results by virtue of their reciprocity. Loss of reciprocity indicates the onset of crack propagation and is indicated by diverging evolutions. This result can be used advantageously to assess not only the influence of characteristic impedance mismatch but also to get an idea of the bulk time to fracture.

Two examples with specific problems have been presented: one (steel) with problems related to uneven crack length and the position of the fracture gages and the other (PMMA) with impedance matching related problems.

It is generally observed that surface fracture gages give a reasonable estimate of the fracture time with respect to the slightly shorter bulk fracture time.

An additional point is that the present approach can complement a deficient gage reading, or even facilitate the testing of materials under severe (temperature, radioactive) environment where gage laying can be hazardous.

Acknowledgement

We wish to acknowledge the valuable contribution of Dr. M. Bulik and Dr. A. Constantinescu to the development of the explicit FE procedures used in this work. We also thank Dr. D. Boussaa for useful discussions.

References

1. L.B. Freund, *Dynamic Fracture*, Cambridge University Press Cambridge (1990).
2. *Crack Dynamics in Metallic Materials*, J.R. Klepaczko (ed.) Springer-Verlag, Wien (1990).
3. J.J. Mason, J. Lambros and A.J. Rosakis, *Journal of the Mechanics and Physics of Solids* 40 (3) (1992) 641–661.
4. H.D. Bui and H. Maigre *Comptes Rendus Académie des Sciences de Paris* tome 306 Série II (1988) 1213–1216.
5. H.D. Bui, H. Maigre and D. Rittel, *International Journal of Solids and Structures* 29 (23) (1992) 2881–2895.
6. D. Rittel, H. Maigre and H.D. Bui, *Scripta Metallurgica et Materialia* 26 (1992) 1593–1598.
7. J.F. Kalthoff and R. Podleschny, in *Proceedings of the International Symposium on Impact Engineering*, I. Maekawa (ed.) (1992) 605–610.
8. H. Maigre and D. Rittel, *International Journal of Solids and Structures* 30 (23) (1993) 3233–3244.
9. H. Kolsky, *Proceedings of the Physical Society of London* B62 (1949) 676–700.
10. D. Rittel and H. Maigre, in *Proceeding of the Eighth International Conference on Fracture*, Kiev (1993) to appear.
11. H. Wada, *Engineering Fracture Mechanics* 41 (6) (1992) 821–831.
12. K.J. Bathe, *Finite Element Procedures in Engineering Analysis*, Prentice–Hall, Inc., Englewood Cliffs (1982).

13. M. Bulik, *Sur l'optimisation de protections parasismiques*, Doctoral thesis, Universite Paris VI, Paris (1993).
14. P.S. Follansbee, in *Metals Handbook* Vol. 8, 9th edn., ASM, Metals Park (1985).
15. H. Kolsky, *Stress Waves in Solids*, Dover, Inc., New York (1963).
16. S. Aoki and T. Kimura, *Journal of the Mechanics and Physics of Solids* 41 (3) (1993) 413–425.
17. CEA, CASTEM 2000 Object Oriented FE Code, Saclay.
18. M.F. Kanninen and C.H. Popelar, *Advanced Fracture Mechanics*, Oxford University Press, New York (1985).